Geomechanics for Energy and the Environment 6 (2016) 45–57

Contents lists available at ScienceDirect

Geomechanics for Energy and the Environment

journal homepage: www.elsevier.com/locate/gete

Factors influencing collection performance of near surface interseasonal ground energy collection and storage systems

José Javier Muñoz-Criollo, Peter John Cleall *, Stephen William Rees

Cardiff School of Engineering, Cardiff University, Cardiff, CF24 3AA, Wales, UK

HIGHLIGHTS

- Impact of surface boundary, climate and materials on performance is investigated.
- Numerical model is validated and applied with varying system parameters.
- System heat losses are strongly influenced by the performance of insulation layers.
- Reduced amplitude of air temperatures in warmer climates affects collection rates.
- Correct surface boundary conditions are critical in modelling systems dynamics.

ARTICLE INFO

Article history:
Received 31 August 2015
Received in revised form 4 April 2016
Accepted 7 April 2016
Available online 20 April 2016

Keywords:
Ground energy
Thermal
Climate

ABSTRACT

The influence of surface boundary conditions, varying climatic conditions and engineering material parameters on the collection performance of near surface interseasonal ground energy collection and storage systems are investigated. In particular, the performance of a proposed design of an interseasonal heat storage system which has also been investigated by others as part of a full scale demonstration project is considered. A numerical model is developed and validated against field data. It is then applied to undertake a series of simulations with varying system parameters. It is found that (i) higher values of thermal conductivity of the storage layer result in increased storage of thermal energy and lower peak temperatures, (ii) system heat losses are strongly influenced by the performance of insulation layers, (iii) warmer climatic conditions provide more thermal energy available to be stored; however, changes in the amplitude of seasonal air temperature variations have an effect on the rate of collection of thermal energy and (iv) the use of correct surface boundary conditions is critical in modelling the dynamics of these systems.

1. Introduction

The use of the ground as a reservoir or source of thermal energy is long established. In recent times, systems utilising modern engineering materials and technology have become more widespread, examples include ground source heating (e.g. Ref. [1]), shallow energy piles (e.g. Ref. [2]), passive heating and cooling of buildings (e.g. Refs. [3,4]) and inter-seasonal thermal energy storage (e.g. Ref. [5]).

The performance of near surface ground energy collection and storage systems is highly dependent on the spatial and temporal variation in the amount of energy present in the near-surface region of the soil as well as the specific design and operation characteristics of the system. Inter-seasonal heat storage systems are of use in applications that have a cyclical annual thermal energy demand typically driven by energy demands in the winter that may be met by using excess heat energy stored in the summer. In some cases, waste heat may be captured from heating and ventilation systems. Applications include heating of buildings, winter maintenance of highways and minimising ice formation at aircraft stands.

* Corresponding author. Tel.: +44 29 20875795; fax: +44 29 20874004.
E-mail addresses: MunozCriolloJJ@cf.ac.uk (J.J. Muñoz-Criollo), Cleall@cardiff.ac.uk (P.J. Cleall), ReesS@cardiff.ac.uk (S.W. Rees).

http://dx.doi.org/10.1016/j.gete.2016.04.001

The ability to model such facilities offers potential benefits at the design stage, in particular for scenario testing to help optimise the system. However, for a model to be representative it must be capable of simulating the transient temperature regime in the surrounding soil with reasonable precision. To this end, a significant body of research has appeared in the literature. For example, Ma et al.[6] implemented a 2D heat transfer FEM model to obtain soil temperature profiles suitable to be used as initial conditions in problems involving heat and mass transfer in soils. Quin et al.[7] presented a detailed algorithm for the computation of soil surface heat fluxes and temperature changes using a complete description of the surface energy balance under bare soil conditions. Their model was validated against experimental measurements using publicly available meteorological data for a desert in southern Israel. Rajeev et al.[8] developed a 1D numerical model to describe the ground–atmosphere interaction and soil moisture and temperature profiles to a depth of 2 m below ground surface over a period of 2 years. Their model was validated with data measured at a site in Melbourne, Australia and meteorological data was obtained from a station installed on-site. Liu et al.[9] used a simplified 1D model that estimated the soil surface temperature as a function of air temperature measured close to the soil surface. They predicted underground temperature profiles over a summer season in Nanjing, China.

In the context of the numerical analysis, the methods and assumptions employed vary depending on the specific physical characteristics of the problem in hand. For example, Yumrutaş et al.[10] developed a semi-analytic model to investigate the annual periodic performance of a cooling system which coupled a chiller with a spherical underground thermal energy storage element. Shang et al.[11] studied the temperature recovery of the ground surrounding a relatively deep (50 m vertical U-tubes) ground-source heat pump under intermittent operation. Several influencing factors were taken into account including the soil thermal conductivity, air temperature and solar radiation. Wu et al.[12] assessed the performance of a shallow (1.2 m depth) horizontal slinky ground source heat exchanger under UK (Oxfordshire) weather conditions. A 3D numerical model was validated with experimental measurements collected over a 2 month period using soil thermal properties measured from in situ undisturbed soil samples. The model was then used to study the impact of varying pipe diameters and slinky interval distances. Esen et al.[13] developed a 2D numerical model to evaluate a shallow (1 m depth) ground-coupled heat pump system designed for space heating. They validated the numerical model using experimental measurements[14] and measured soil thermal properties. Congedo et al.[15] performed a set of 3D numerical simulations to study the performance of shallow (1 m depth) horizontal ground heat exchangers under varying pipe distributions, heat carrier fluid velocities, pipe depths and soil thermal properties. It was concluded that most important parameter for the heat transfer performance of the system was the soil thermal conductivity with higher values (1, 2 and 3 W/m K considered by the authors) delivering a better performance. Ramírez-Dávila et al.[16] studied the performance of a relatively shallow earth-to-air heat exchanger (10 m depth) under three different types of weather in Mexico: desert (Cd. Juárez, Chihuahua), mild weather (México city) and hot-humid weather (Mérida,Yucatán). It was found that the performance of the system is dependent on the weather conditions and the season under which it operates.

For effective assessment and design of ground energy collection and storage systems, and in many geomechanical environmental and energy related applications, it is necessary to be able to correctly represent a number of key factors. These include (i) the transfer of heat between the ground surface and the atmosphere, (ii) the movement of heat within the engineered soil mass and (iii) the movement of heat energy within the collector and storage systems. This paper explores how the performance of interseasonal heat storage systems may be affected by meteorological conditions, surface flux boundary conditions, and the thermal properties of the storage materials. It appears that these factors have not been fully explored and so the objective of the paper is to investigate and quantify these three factors via a series of numerical analyses of a typical system. To this end, a numerical framework is developed and validated against a comprehensive dataset produced by others.[5] The impact on system performance is assessed in terms of soil temperature profiles and thermal energy stored.

2. Modelling framework

The analysis of thermal problems usually requires the solution of the transient heat transfer equation for a 2D or 3D soil domain. This may be coupled with the solution of the transient heat advection equation (in 3D) or a suitable mathematical algorithm able to represent the transfer of heat in the soil–pipe–fluid system in 2D. In both cases, suitable boundary conditions are required to represent both energy balance at the soil surface and energy transfer between the soil mass and the pipes. In the present study, the mathematical framework for a 2D case is presented (full details are given in Ref. [17]). In order to simplify the analysis, only heat transfer by conduction is considered in the soil mass while other physical processes like convection and mechanical deformation are neglected.

Since the current model addresses the performance of a near-surface thermal device, the theoretical representation of heat transfer at the soil surface includes several terms that are typically not required in models dealing with systems buried deep into the ground and therefore comparatively insulated from soil–surface interactions. The relative contribution of these flux terms is of course problem dependent but in general terms solar radiation is the most significant followed by infrared radiation and then smaller convective and evaporative heat fluxes.

2.1. Heat transfer

Transient heat transfer, when only conduction is considered, can be expressed as[18]

$$C_{p,b}\frac{\partial T_s}{\partial t} = \nabla \cdot (\lambda_b \nabla T_s) \tag{1}$$

where $C_{p,b}$ (J/m^3 K) is the volumetric heat capacity of the soil, λ_b (W/m K) is its thermal conductivity, T_s (°C) is the

temperature of the soil, t is time, $\nabla\cdot$ is the divergence operator and ∇ is the gradient operator.

2.2. Surface heat fluxes

A general energy balance can be used to define the boundary condition at the soil surface. Taking solar radiation, infrared radiation, convective and evaporative heat fluxes into account the energy balance can be expressed as[19]

$$-\lambda_b \frac{dT_{ss}}{d\hat{n}} = (1-\alpha_S)R + \sigma\varepsilon_{ss}\left(\varepsilon_{sky}T_{a,K}^4 - T_{ss,K}^4\right) + h_E(q_a - q_{ss}) + h_C\left(T_a - T_{ss}\right) \quad (2)$$

where α_S (–) is the solar albedo, $\hat{n}$ is the unitary vector normal to the surface, R (W/m^2) is the magnitude of solar radiation, σ (W/m^2 K^4) is the Stefan–Boltzmann constant, ε_{ss} (–) is the infrared emissivity of the surface, ε_{sky} (–) is the emissivity of the sky,[19] T_a (°C) and $T_{a,K}$ (K) are the temperature and absolute temperature of the air respectively, T_{ss} (°C) and $T_{ss,K}$ (K) are the temperature and absolute temperature of the soil surface respectively, q_a (kg/kg) and q_{ss} (kg/kg) are the specific humidity of air and soil surface respectively, h_E (W/m^2) is the evaporative heat transfer coefficient, and h_C (W/m^2 K) is the convective heat transfer coefficient.

In principle, the surface of the soil can be composed of many regions with different properties that correspond to different types of cover. In this paper three, particular surface types are considered: bitumen pavement, bare soil and soil partially covered by vegetation.

2.2.1. Paved surface and bare soil

For bitumen pavement and bare soil cases, values for variables used and expressions for h_E and h_C in Eq. (2) are taken from Refs. [20,19] respectively.

$$h_E = \rho_a L_V (C_{fc}C_{sh}u + C_{nc}\Delta\theta_v^{0.33}) \quad (3)$$

$$h_C = \rho_a c_{p,a} (C_{fc}C_{sh}u + C_{nc}\Delta\theta_v^{0.33}) \quad (4)$$

where ρ_a (kg/m^3) is air density, $c_{p,a}$ (J/kg K) is the specific heat capacity of air, L_v (J/kg) is the latent heat of vaporisation of water, $\Delta\theta_v$ (K) is the difference in virtual temperature between the air and the soil surface and u (m/s) is the surface wind velocity. The concept of virtual temperature arises in meteorology and is introduced when working with moist air as it allows use of the ideal gas law for dry air.[21] C_{nc} (m/s K$^{1/3}$), C_{fc} (–) and C_{sh} (–) are coefficients that weight the natural and forced convective processes and the sheltering caused by surrounding objects respectively. It is assumed that the paved surface is impervious and that any water will run-off, as such the contribution of evaporation has been neglected and only natural and forced convection are considered. Evaporation from the soil surface is considered and a soil surface water tension equal to the average of the saturation and wilting point values is assumed.

2.2.2. Soil covered by vegetation

Where the soil is covered by vegetation, the approach used to consider energy balance is modified to take into account the presence of a canopy cover using the model described in the works of Deardorff[22] and Best,[23] and applied as suggested by Herb et al.[19] who also provides suitable values for variables and coefficients present in Eq. (2). The consideration of the heat transfer interactions of the canopy layer results in an additional heat balance equation that is coupled to the heat balance equation for the soil surface. The latter is given as

$$\begin{aligned}-\lambda_b\frac{dT_{ss}}{dx} &= (1-\alpha_s)(1-\nu)R \\ &+ \left[\sigma\varepsilon_{ss}\left((1-\nu)\varepsilon_{sky}T_{a,K}^4 - T_{ss,K}^4\right)\right. \\ &\left. + \nu\varepsilon_c\sigma T_{c,K}^4\right] + h_E(1-C_e\nu)(q_a - q_{ss}) \\ &+ h_C(1-C_e\nu)(T_a - T_{ss}) \end{aligned} \quad (5)$$

where ν (–) is the canopy density, $T_{c,K}$ (K) is the absolute temperature of the canopy cover, ε_c (–) is the canopy emissivity and the constant C_e (–) establishes the level of soil evaporation for fully dense canopies. The heat balance equation for the canopy cover (which is assumed to have negligible heat capacity) is given by

$$\begin{aligned}0 &= (1-\alpha_c)\nu R + \nu\sigma\varepsilon_{ss}\varepsilon_{sky}T_{a,K}^4 \\ &- 2\nu\sigma\varepsilon_c T_{c,K}^4 + \nu\sigma\varepsilon_{ss}T_{ss,K}^4 \\ &+ \frac{\rho_a L_v \nu}{r_{a,c}+r_s}(q_a - q_{sat}) + \frac{\rho_a c_{p,a}\nu}{r_{a,c}}(T_a - T_c) \end{aligned} \quad (6)$$

where α_c (–) is the canopy solar albedo, T_c (°C) is the temperature of the canopy cover, q_{sat} (kg/kg) is the saturation specific humidity of the canopy cover,[21] $r_{a,c}$ (s/m) is the aerodynamic resistance for the canopy cover and r_s (s/m) is the stomata resistance calculated as

$$r_{a,c} = \frac{1}{0.01(0.3+u)} \quad (7)$$

$$r_s = 200\left(\frac{R_{\max}}{R+0.03R_{\max}} + \left(\frac{\theta_{wp}}{\theta}\right)^2\right) \quad (8)$$

where $R_{\max}$ (W/m^2) is the maximum solar radiation, θ (m^3/m^3) is the moisture content and θ_{wp} (m^3/m^3) is the wilting point soil moisture.

2.2.3. Diurnal shading

The effect of shading due to nearby surface features (e.g. trees or buildings) on the surface temperature of a paved surface has been taken into account by modifying the solar radiation term to include a factor to account for the impact of shading[24]:

$$R_d = RD_s \quad (9)$$

where R_d (W/m^2) is the effective solar radiation and D_s (–) is a diurnal shading factor which can be defined to be a function of both time and surface location.

2.3. Heat transfer within storage and collector pipes

In this paper, the case of a pipe running perpendicular to the 2D plane flow domain representing the soil is considered, as illustrated in Fig. 1. Following the typical

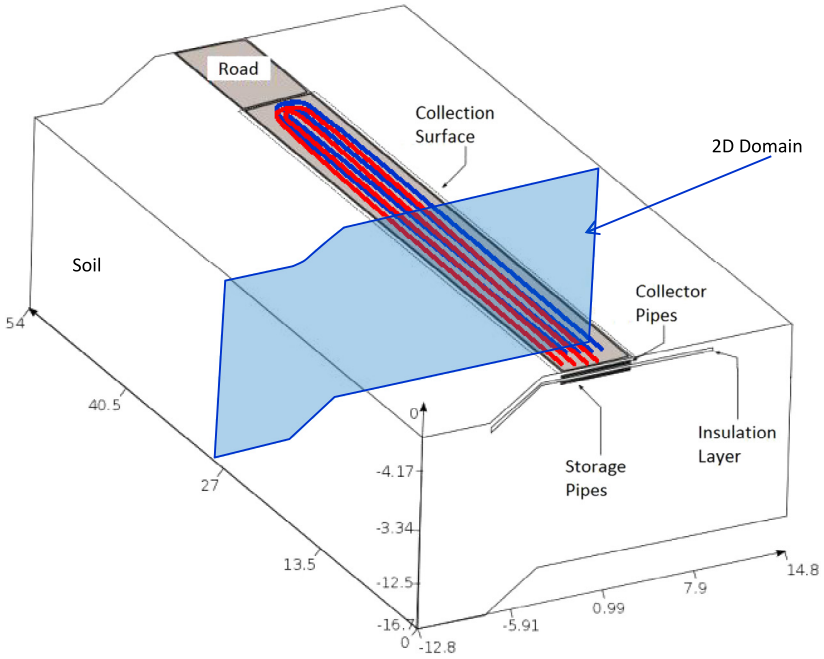

Fig. 1. Schematic of interseasonal heat storage system, dimensions in (m).

mathematical description used to describe heat exchangers (e.g. Ref. [18]), the energy transferred between a unit length of an idealised pipe perpendicular to the plane of a 2D plane flow domain and the surrounding soil, q_p (W/m^2), is calculated as

$$q_p = U_p \left(T_s - T_f\right) \tag{10}$$

where T_s (°C) is the temperature of the soil in direct contact with the pipe. U_p (W/m^2 K) is the overall heat transfer coefficient of the pipe and is a function of the pipe geometry, fluid velocity and material properties of the pipe and fluid. T_s is calculated as the average value of all the degrees of freedom at the soil–pipe boundary. T_f is estimated as the average of the inlet and outlet temperatures of the idealised pipe, in which heat transfer along the direction of the fluid flow can be described as

$$q_p = \varepsilon_p c_{p,f} \dot{m}_f (T_s - T_{f,i})/A_p \tag{11}$$

where $c_{p,f}$ (J/kg K) is the specific heat capacity of the pipe fluid, $\dot{m}_f$ (kg/s) is the mass flow inside the pipe, $T_{f,i}$ (°C) is the temperature at the inlet of the idealised pipe, A_p (m^2) is the area through which the heat is being transferred and ε_p is the heat exchanger thermal efficiency that can be defined as[18]

$$\varepsilon_p = 1 - \exp\left[-\frac{U_p A_p}{\dot{m}_f c_{p,f}}\right]. \tag{12}$$

Eq. (11) implies that the soil temperature at any time step remains constant for the whole length of the assumed pipe, this assumption is a necessary limitation of the adopted 2D modelling approach. When two or more pipes perpendicular to the domain form a closed system, the estimated outlet temperatures of a pipe or set of pipes can be used as inlet temperatures for the remaining set of pipes closing the system and analysed in an iterative manner.

2.4. Stored thermal energy

In this paper, the thermal energy collected per unit depth by an interseasonal heat storage facility is used as a parameter to compare its performance under varying conditions of selected variables. The additional thermal energy contained in a defined region E (W/m) is calculated as[25]

$$E = C_{p,b} \int_{sr} \Delta T_{sr} dA_{sr} \tag{13}$$

where ΔT_{sr} (°C) is the temperature difference in the region under consideration (e.g. *Storage Region*, Fig. 2) due to the active system in comparison to a case without the activation of the system and A_{sr} (m^2) is the area of the region.

2.5. Numerical solution

A numerical solution of the 2D model has been developed using the finite element method (Galerkin weighted residual) to solve the transient heat transfer (Eq. (1)) with boundary conditions as described in Section 2.2. Time discretisation is achieved following Rothe's method via a Crank–Nicholson scheme. The open source and publicly available finite element library Deal.ii is used to implement the numerical method and solve the system of equations.[26]

In order to calculate the surface heat flux in each time step, the heat balance equations at the soil surface as defined by Eq. (2) for bare soil conditions and pavement and by Eqs. (5) and (6) for a soil covered with vegetation are solved using Newton's method, as suggested by Deardorff,[22] since they are non-linear due to the infrared and evaporative heat transfer fluxes. In particular for the

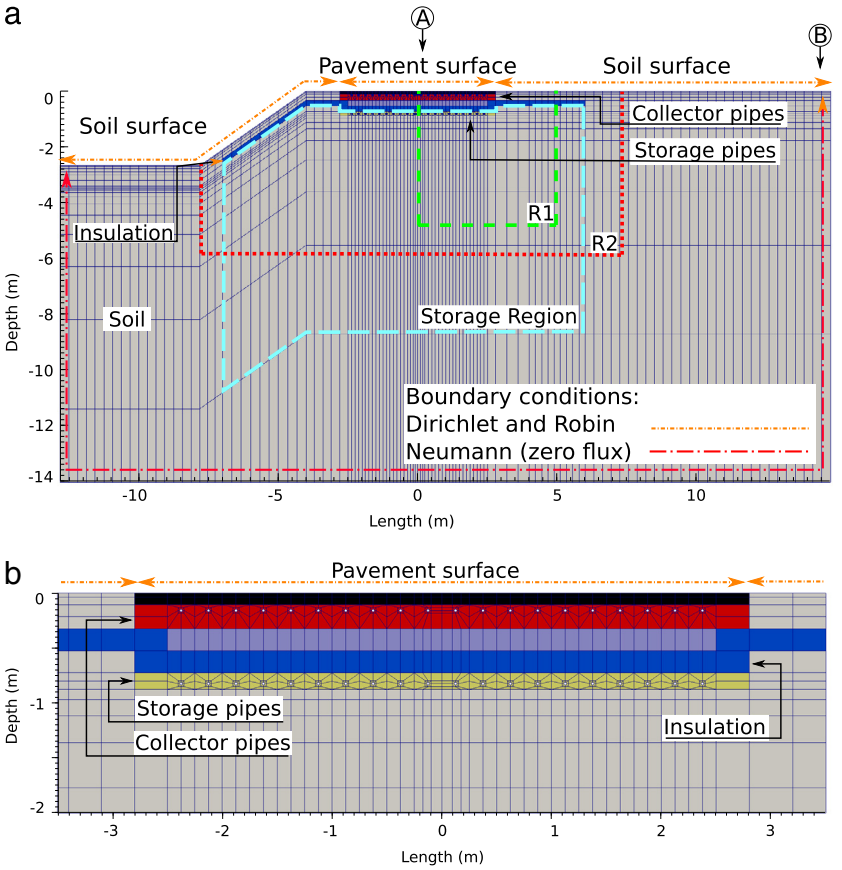

Fig. 2. (a) Cross-section of interseasonal heat storage system. (b) Close up of collector and storage pipes region.

case of vegetative cover, Eqs. (5) and (6) are solved iteratively by estimating a canopy temperature and then calculating the corresponding ground surface heat flux and solving Eq. (1).

An algorithm that takes into account two interconnected pipe heat exchangers is developed to estimate the temperature at the outlet of the first heat exchanger pipe using Eq. (11) that in turn is used as temperature at the inlet of the second pipe. The total amount of energy transferred between the two heat exchangers and the soil is calculated iteratively using Eq. (10). Full details and validation of this approach to modelling thermal soil–pipe–fluid interactions are available in Ref. [17].

3. Case study: interseasonal heat storage system

The design of the system considered in this paper is based on the interseasonal heat storage facility investigated by Carder et al.[5] as part of a full scale demonstration project. It consists of a collector pipe array (5 m wide and 30 m long, using 10 polyethylene pipes spaced at 0.25 m centres and arranged in horizontal U loops) placed at a depth of 0.1 m below a road surface and a second similar storage pipe array at a depth of 0.875 m, below a 0.2 m thick insulation layer, as illustrated in Figs. 1 and 2. The extent of the insulation layer and the position of collector and storage pipes are indicated. For clarity further material layers composing the road structure (detailed in Table 1) are not shown. Full details can be found in Ref. [5] and Ref. [17]. Additionally, three sub-regions labelled as R1, R2 and Storage Region and two points A and B used in the analyses presented in Sections 4 and 6 are shown. Fig. 2(b) shows a close-up of the region containing the collector and storage pipes.

The purpose of an interseasonal heat storage system is to take advantage of the difference in thermal energy available between seasons. One possibility is the collection of heat in the summer months to be used at appropriate times during winter months. Under these circumstances the system is activated (i.e. pumps switched on) whenever the temperature difference between the collection and storage pipes is higher than a certain value and is stopped when it drops below another (not necessarily the same) value. In this paper the criteria for activation and deactivation of the collector system follow those suggested by Carder et al.[5] who set the activation of the system when the temperature difference between the control sensors located at the collector and storage levels reached approximately 1.4 °C. Once active, the system was turned off when the temperature difference dropped to approximately 0.3 °C.

4. Validation

Validation of the model is addressed here via simulation of the above demonstration project. The system design and

Table 1
Material parameters.
Source: All from Ref. [5], except for 'Near ideal insulation'.

Material type	Density (kg/m^3)	Specific heat (J/kg K)	Thermal conductivity (W/m K)	Thickness (m)
Asphalt	2400	850	0.85	0.105
Concrete	2100	840	1.4	0.055
Silty clay	1960	840	1.21	14
Backfill	840	840	1.21	0.5
Polystyrene insulation	30	1130	0.034	0.2
Sand	2240	840	0.33	0.150
Near ideal insulation	30	1130	0.00034	0.2

activation and deactivation criteria used in the demonstration project are as described in Section 3. Meteorological data measured on site, provided by Carder et al.,[5] is used to consider the performance of the system during a 2.5 month collection period.

The simulation is undertaken in a series of sequential steps. Initially, a preliminary simulation consisting of 8 yearly cycles (each using meteorological data from August 2005 to August 2006) is undertaken to establish suitable initial conditions (Period 1). These initial conditions are then used to simulate from May 2005 to August 2005 after installation of the system but before its activation (Period 2), during this period the soil in the storage region is largely prevented from natural warming due to the presence of the insulation layer (for brevity results from this analysis are not shown here but are very similar to those presented in Fig. 9(a)). Finally, a collection period (Period 3) where the system was activated for a first collection stage (from the end of August 2005 until the beginning of November 2005) is simulated. The mesh used for the numerical analysis is shown in Fig. 2 and is made up of 2452 four node isoparametric linear elements (4 temperature degrees-of-freedom per element). After checks on both spatial and temporal convergence Periods 1 and 2 are simulated using hourly time steps, while in Period 3 a 15 min time step is used. Far field boundary conditions and bottom boundary conditions are assumed as insulated (zero flux). Boundary conditions at the surface are set using Eqs. (2)–(4) for the paved surface and Eqs. (5) and (6) for the soil surface, which is assumed to be partially covered by vegetation based on field observations. A schematic representation of the boundary conditions used for the problem is presented in Fig. 2. Analysis of a far field control borehole found a canopy density (ν) of 0.85 and an average level of shading of 0.5 to be suitable.[17] Reference values for thermal material properties considered in the domain are taken from Ref. [5] and listed in Table 1, coefficients and constants used in the theoretical description of the heat transfer process are given in Table 2. Pipe fluid velocity and composition are also based on typical values reported by Carder et al.[5] Fig. 3(a) and (b) show the numerical results obtained compared with experimental measurements at collector pipes depth and storage pipes depth respectively. It can be seen that the temperatures calculated by the numerical model proposed are in good agreement with the measured data. Statistical analysis of the simulated results and the measured data for the whole collection period yields a root mean square error value of 1.09 °C in the collector region and 0.38 °C in the storage region. This validation of the modelling approach for heat collection and storage builds confidence to allow further exploration of the impact of various system parameters.

Table 2
Coefficients and constants used in analyses.

λ_b (W/m °C)	1.2	C_{nc} (m/s K$^{1/3}$)	0.0015
α_s	0.15	C_{sh}	1
α_c	0.15	C_{pf} (J/kg K)	4091.41
σ (W/m^2 K^4)	5.67E−8	$c_{p,a}$ (J/kg K)	1012
ε_{ss}	0.95	ν	0.85
ρ_a (kg/m^3)	1.2041	C_e	0
L_v (J/kg)	2.45E6	ε_c	0.95
C_{fc}	0.0015	R_{max} (W/m^2)	1000
θ	0.24	θ_{wp}	0.12
D_s	0.5	U_p (W/m^2 K)	192
A_p (m^2)	2.17	$\dot{m}_f$ (l/s)	0.155

5. Numerical investigation

The main objective of this paper is to explore the impact that the variation of certain factors have on the thermal performance of interseasonal heat storage devices, specifically, in terms of the thermal energy collected and the temperature profiles obtained after a collection period. As above, in the validation section, these simulations consist of three steps: (i) an 8-yearly-cycle pre-analysis performed in order to obtain steady state initial conditions (Period 1), (ii) an analysis after installation of the system at the beginning of summer (Period 2), and (iii) an analysis of the active system with the system active for ∼3 months (84 days) from the beginning of autumn (Period 3).

Three sets of simulations are performed, each exploring the influence of a particular system variable on performance. In each set of simulations the same base case analysis is performed using meteorological data generated for mild climatic conditions, a soil surface boundary condition that includes a vegetative cover and a thermal conductivity of 1.2 W/m K in the storage region under the insulation layer. The mesh, time steps and far-field and bottom boundary conditions are as described in the validation section. The specific simulations undertaken and details of the base case conditions are defined in the following sections.

5.1. Variation in thermal conductivity (Simulations 1–4)

The influence of varying the thermal conductivity values employed in the Storage Region (shown in Fig. 2(a)) is explored via a simple parametric study. A base case value of 1.2 W/m K has been assumed (*Base case*/*Simulation* 1) and two additional values of 0.96 W/m K (*Simulation* 2) and 1.44 W/m K (*Simulation* 3) are also considered. These variations could arise in practice as a result of the process of

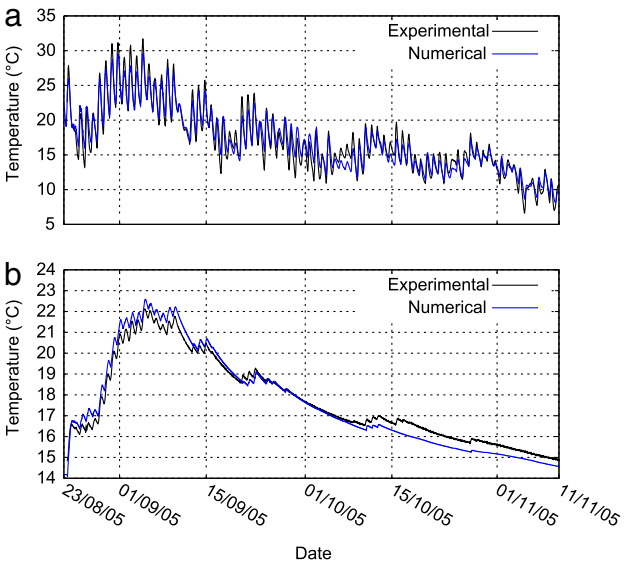

Fig. 3. Experimental and numerical temperature transients at (a) collector depth (0.1 m) and (b) storage depth (0.875 m) for the first activation period reported by Carder et al.[5].

installation of the system or from disrupting the natural cycles of wetting and drying since the insulation is likely to be relatively impermeable to water. A further analysis of the base case but with a near-ideal insulation layer is also considered (*Simulation* 4), material parameters used for this layer are given in Table 2. Simulations of Periods 1 and 2 in this section are run using the base case conditions, while in Period 3 the particular value of conductivity under consideration is employed. The change in soil thermal properties between Period 2 and 3 is done in order to simplify comparisons between the analyses by having common initial conditions, it is recognised however that this is a limitation and a potential source of error in the analysis due to an imbalance between the temperature field within the ground and its thermal properties.

5.2. Assumed climatic conditions (Simulations 5–9)

The meteorological conditions used for the numerical simulations performed in this section are generated using two analytical expressions (detailed in the Appendix) for air temperature and solar radiation proposed by Cleall et al.[25] based on experimental observations as part of the development of analytical solutions for temperature profiles and thermal energy stored in the ground.

It is hypothesised that the performance of an inter-seasonal heat storage device is likely to be influenced by the type of weather conditions under which it operates. For this reason, three types of climatic conditions are explored:

- Mild (*Base case*/*Simulation* 5)—Obtained from the British Atmospheric Data Centre (BADC 2014) for the years 2004 and 2005 for Toddington, UK.[27]
- Cold (*Simulation* 6)—Obtained from the Icelandic Meteorological Office for the years 2004 and 2005 for the city of Reykjavík, Iceland.

Table 3
Coefficients used in air temperature and solar radiation analytical expressions (14) and (17) for three different climates.

Coefficient	Mild weather	Cold weather	Hot weather
A	241.5 W/m^2	218.3 W/m^2	260.8 W/m^2
B	19.6 W/m^2	1.6 W/m^2	167.8 W/m^2
C	18.4 °C	11.2 °C	29.9 °C
D	6.4 °C	−0.2 °C	24.7 °C
E	9.8 °C	5.0 °C	8.2 °C
F	6.3 °C	9.8 °C	9.6 °C

- Hot (*Simulation* 7)—Obtained from the meteorological station of the School of Engineering of the Autonomous University of Yucatán for the year 2009 for the city of Mérida, México.

Using these datasets the values of the coefficients present in Eqs. (15) and (16), and in Eqs. (18)–(21) were calculated and are listed in Table 3. The meteorological data produced with Eqs. (14) and (17) were used for all simulation periods and are illustrated in Figs. 4 and 5 (half yearly cycles of daily maximum solar radiation, and maximum and minimum temperatures are shown). Values for wind speed and relative humidity were fixed at 1.14 m/s and 80.6% respectively for simplicity based on the meteorological data measured on site by Carder et al.[5] in a location close to Toddington, UK. Two additional analysis are performed to investigate the impact of the amplitude of temperature variation by replacing coefficients *E* and *F* (which represent the mid-summer average amplitude, and mid-winter average amplitude respectively) for the mild climatic conditions with the corresponding coefficients of cold (*Simulation* 8) and hot conditions (*Simulation* 9).

5.3. Surface conditions (Simulations 10–12)

Typically two different approaches are applied to consider soil–atmosphere thermal interactions. The simpler, in terms of application, is the use of a fixed (Dirichlet)

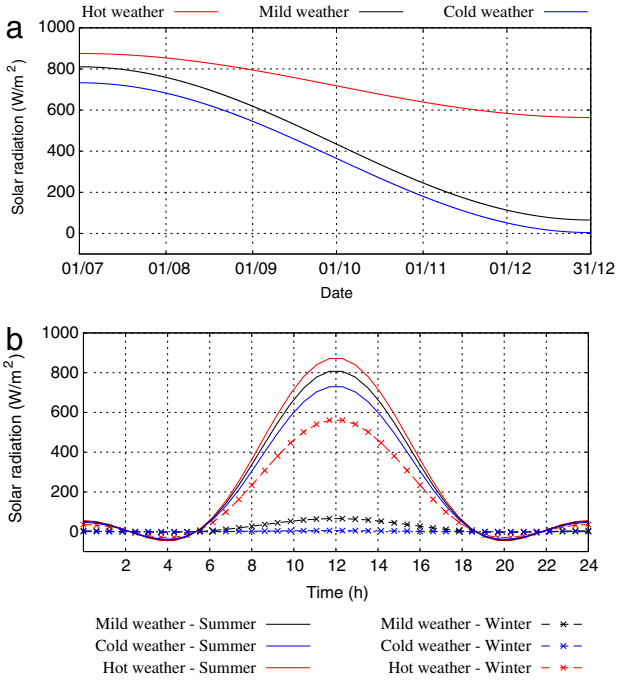

Fig. 4. Solar radiation profiles obtained with Eq. (14) and coefficients listed in Table 3. (a) Seasonal variation of peak daily values from summer (July 1st) to winter (December 31st) for three climates considered. (b) Daily variation in summer (July 1st) and winter (December 31st).

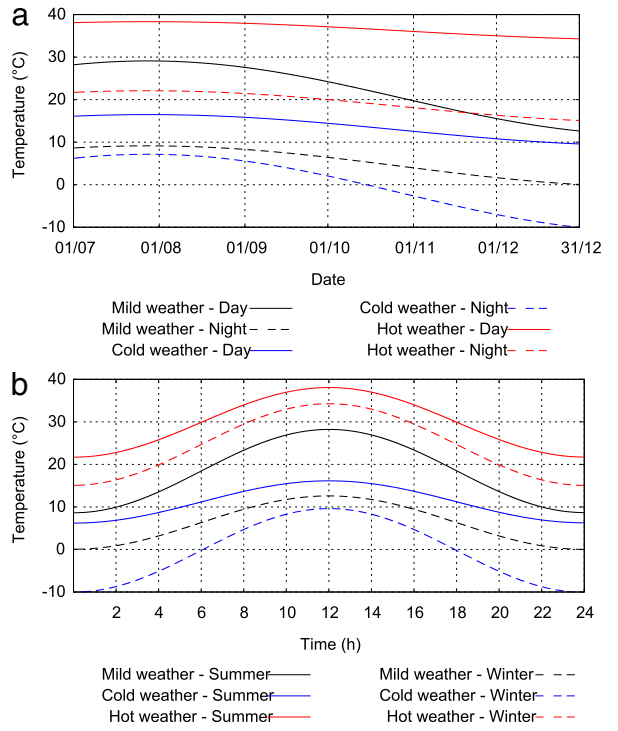

Fig. 5. Air temperature profiles obtained with Eq. (17) and coefficients listed in Table 3. (a) Seasonal variation at day (noon) and night (midnight) from summer (July 1st) to winter (December 31st) for three climates considered. (b) Daily variation in summer (July 1st) and winter (December 31st).

boundary condition based on measured or estimated temperatures to define the variation of temperature of the soil surface (including any pavement) with time. In many cases, this is approximated to near surface air temperatures as these are often readily available. In this study, the air temperature defined by Eq. (17) is used (*Simulation* 10).

A more complex, but more physically representative, approach is to apply a third kind (Robin) boundary

condition which allows representation of the surface fluxes defined in Section 2.2. In this study, two sets of boundary conditions have been utilised for the soil surface (not covered by pavement):

- Bare soil (*Simulation* 11). Eq. (2) is used to define the surface energy balance with Eqs. (3) and (4) representing the heat transfer coefficients for evaporation and convection respectively.
- Soil covered by vegetation (*Base case*/*Simulation* 12). Eqs. (5) and (6) are used to represent energy balance between the soil and canopy cover. The heat transfer coefficients for evaporation and convection are as defined by Eqs. (3) and (4).

The flux boundary condition applied to the soil surface covered by pavement in *Simulations* 11 and 12 is given by Eq. (2), using Eq. (4) to define the heat transfer coefficient for convection.

6. Results and discussion

Variations in thermal conductivity

Simulations 1–3 study the effect of varying the thermal conductivity in the storage region under the insulation layer. To observe the influence of the active system, temperatures for Period 3 are obtained both with and without collector system activation. The difference in these temperatures indicates the area of influence of the system in isolation from temperature variations due to meteorological and surface conditions. Fig. 6 shows the temperature differences obtained in the region marked as R2 in Fig. 2(a) at the end of Period 3 for *Simulations* 1–3. It can be seen that higher temperature differences near the storage pipes are obtained for the case with low thermal conductivity while in turn a wider area of influence approaching the edge of the insulation layer is obtained with higher thermal conductivities.

Fig. 7(a) shows the variation in time of thermal energy stored in the Storage Region calculated using Eq. (13). Fig. 7(b) and (c) show the soil temperature variation at collector depth (0.1 m) and storage depth (0.875 m) respectively. Fig. 7 also includes results from *Simulation* 4 using a near-ideal insulation layer for the base case. Thermal energy contained in the Storage Region starts to rise at the beginning of Period 3, reaches a maximum at day 42 and then decreases until the end of the simulation period is reached. In general, the accumulated thermal energy increases with thermal conductivity this is due to main two factors, firstly heat energy moves away from the pipes more easily to the wider storage mass and secondly this greater movement of heat results in lower soil temperatures at the soil–pipe interface and subsequently a higher thermal gradient across the interface and a higher heat flux. After day 42 the temperature difference between collector and storage no longer satisfies the activation criteria as climatic conditions cool and the temperature in the storage region increases. The subsequent decrease in thermal energy observed up until the end of the simulation period is due mainly to losses through the insulation layer. This is explored in *Simulation* 4 and it can be seen that about 20% more energy could be stored if these

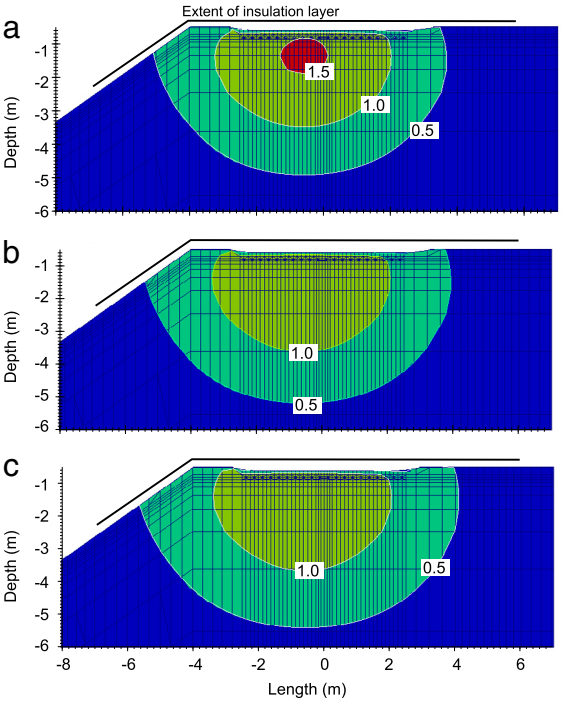

Fig. 6. Temperature difference (°C) contours in region R2 at the end of simulation Period 3 for three thermal conductivities: (a) 0.96 W/m K, (b) 1.2 W/m K and (c) 1.44 W/m K.

losses are minimised. Similar percentages are obtained for the 0.96 and 1.44 W/m K thermal conductivity cases. The temperature profiles at collector depth show negligible differences for the three analysed cases. However, at storage depth it can be seen that higher temperatures are maintained throughout the duration of the numerical simulation for the case with the lowest value of thermal conductivity (0.96 W/m K) in the Storage Region. This behaviour is due to the heightened concentration of thermal energy in the area close to the storage pipes (as shown by Fig. 6) caused by the reduction in thermal energy transfer into the remaining storage region. The opposite is true for the case with higher thermal conductivity (1.44 W/m K). In Fig. 7(c), the effect of a near-ideal insulation layer on the temperature at storage pipes depth can be observed with reduced thermal losses resulting in an increase in temperature towards the end of the simulation period.

Varying climatic conditions

Simulations 5–9 investigate the effect of different climatic conditions on the thermal performance of an interseasonal heat storage facility. Fig. 8 shows the thermal energy accumulated in the storage region during system activation in Period 3. It can be seen that the amount of energy collected in the storage region increases as the climatic conditions become warmer (cold to mild). However, it can also be seen that under hot climatic conditions the energy storage rate differs, being relatively slower at the beginning of the simulation period. This is believed to be related to the annual variation in air temperature as indicated by coefficients *C* and *D* (mid-summer daily average, mid-winter daily average) presented in Table 3. Under

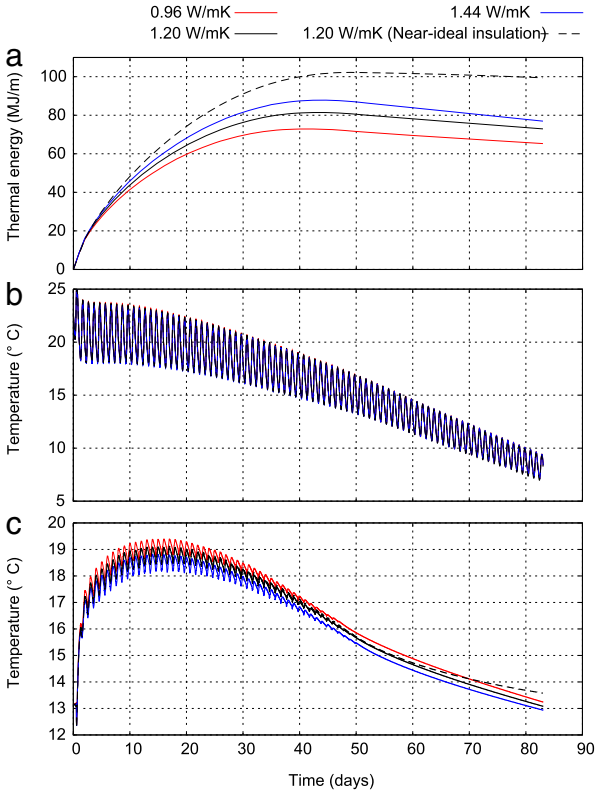

Fig. 7. (a) Variation in time of thermal energy in region R2 for simulation Period 3 for three thermal conductivities and under near-ideal insulation conditions. (b) Corresponding temperature transients at collector depth (0.1 m) and (c) at storage pipes depth (0.875 m).

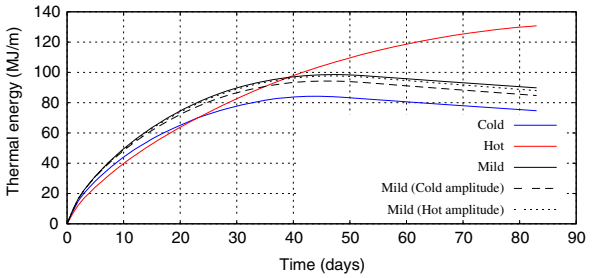

Fig. 8. Variation in time of thermal energy accumulated in the storage region under different climatic conditions.

hot climatic conditions the variation of air temperature between seasons is ∼5 °C while under cold and mild climatic conditions it is ∼11 °C and ∼12 °C respectively. This combined with the placement of insulation at the beginning of summer preventing the soil from naturally warming during the summer months allows a higher thermal gradient for the cold and mild conditions compared with hot conditions. However, this same seasonal variation prevents the system from collecting more thermal energy beyond day 42 as weather conditions cool with this change being more pronounced under cold and mild conditions. In a hot environment, although the weather conditions become cooler in winter, the change is smaller allowing the system to remain active and collect more energy during the whole simulation period. The results of *Simulations* 8 and 9 which explore the influence of the average air temperature amplitudes during summer and winter are shown in Fig. 8. It can be seen that in general, higher summer air temperature amplitudes have a positive impact on the amount of energy that an interseasonal heat storage system is able to collect. However, the levels of thermal energy are still comparable.

Different soil surface conditions

The effect of different boundary conditions at the soil surface is considered in *Simulations* 10–12. Fig. 9 shows temperature contours in the region R1 (Fig. 2(a)) at 0:00:00 h (end of Period 2/beginning of Period 3) on the day of system activation for the three different boundary conditions applied at the soil surface. The three temperature contours show significant differences, for example at the 5 m depth the vegetative cover case (Fig. 9) simulates an almost homogeneous temperature of approximately 11 °C while the corresponding temperature

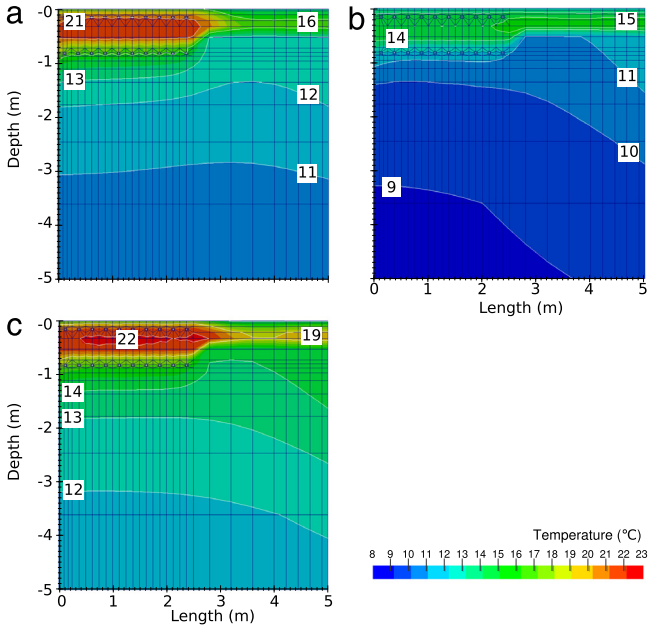

Fig. 9. Temperature contours for region R1 at the beginning of simulation Period 3 using three different boundary conditions at the soil surface: (a) soil surface flux including vegetation cover model (*Simulation* 12), (b) fixed surface temperature (including pavement surface) defined by Eq. (17) (*Simulation* 10), (c) soil surface flux based on bare soil model (*Simulation* 11).

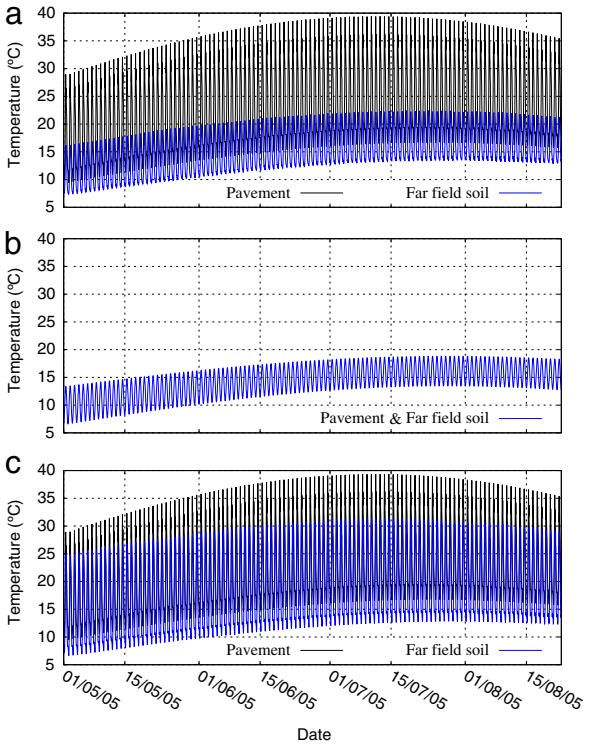

Fig. 10. Surface temperatures at points A (Pavement) and B (Far field soil) for Period 2: (a) soil surface flux including vegetation cover model (*Simulation* 12), (b) fixed surface temperature (including pavement surface) defined by Eq. (17) (*Simulation* 10), (c) soil surface flux based on bare soil model (*Simulation* 11).

under bare soil conditions (Fig. 9(c)) is closer to 12 °C. Under fixed conditions, the temperature at this depth (Fig. 9(b)) is not homogeneous varying between 9 °C and 10 °C. Surface temperature evolution at the centre of the pavement (Point A) and at the far right hand side of the domain (Point B) during period 2 are shown in Fig. 10. At

the surface it can be seen that higher temperatures are obtained in the road section for both canopy covered and bare soil conditions (with the latter being higher), whereas for fixed conditions the temperatures are homogeneous (as expected). It is apparent that using suitable surface boundary conditions is of importance with significant differences in temperature fields obtained. It is worth noting that in the validation exercise, presented in Section 4, use of the more complex flux boundary condition to consider soil–atmosphere thermal interactions was necessary to correctly represent the observed behaviour. A key point here is that, whilst air temperature data is readily available (from meteorological records) and surface type can be spatially defined, records of field measured soil–surface temperatures are much scarcer and require real-time measurement during a systems use. There is therefore a significant benefit in being able to predict soil surface temperatures rather than needing to define them *a priori* before any analysis.

7. Conclusions

In this paper, the influence of varying selected parameters (store thermal conductivity, climatic conditions and surface boundary conditions) on the performance of interseasonal heat storage systems has been investigated. The impact of different values of thermal conductivity in the storage region (affected by the installation process or prevention of natural wetting–drying process) is to reach higher temperatures close to the storage pipes (for low values of soil thermal conductivity) or an increased area of thermal influence (for higher values of soil thermal conductivity). In general higher values of thermal conductivity produce a higher amount of thermal energy being collected in the storage region. Despite this, however, the higher temperatures obtained close to the storage pipes for low thermal conductivities, might facilitate the extraction process or be more adequate for certain thermal applications. Subsequently, it can be concluded that the trade-off between total amount of thermal energy and temperature gradient needs to be optimised to the application under consideration.

Heat losses through a horizontal insulation layer have been found to be as high as 20% of the total thermal energy stored by the system. Higher thermal gradients near the insulation layer will increase these losses, while an increased storage area would require modifications to the insulation layer in order to decrease thermal energy lost through the edges. It is noted that use of innovative materials and systems where material properties can be controlled could lead to significant improvements in the system efficiency and these possibilities are currently under investigation.

The results under different climatic conditions have shown, as might be expected, that in general warmer weather conditions provide more thermal energy for potential storage. However, it was also observed that the seasonal variation of average air temperature has an effect on the rate of collection of thermal energy due to the temperature difference between the soil in the storage region and the air temperature. This effect is heightened if an insulation layer, which prevents natural warming of the soil underneath, is present keeping it close to winter temperatures.

The impact of using different boundary conditions applied on the soil surface has also been investigated. Two Robin-type boundary conditions have been compared, one including the presence of a layer of vegetation on the soil surface while the other assuming the soil as a bare surface. An additional boundary modelling technique has been considered by fixing the surface of the soil (including the paved surface) to the air temperature defined by a time varying mathematical expression. Using these approaches to obtain suitable initial conditions in the simulation periods before the activation of the interseasonal heat storage system have shown that the differences in temperature profiles (and thermal energy) generated in the soil domain are significant and that use of correct surface boundary conditions is critical in modelling the dynamics of the system under consideration.

Whilst it is recognised that the investigation undertaken here is limited to a particular system configuration, it is clear that it can be concluded that the performance of interseasonal heat storage systems is significantly affected by the meteorological conditions, surface flux boundary conditions and the thermal properties of the storage materials and that their correct representation is critical in both the assessment and design of such systems.

Acknowledgements

The authors gratefully acknowledge the support given to the first author whose Ph.D. studies were funded by CONACYT (the Mexican National Council of Science and Technology) and SEP (Mexican Secretariat of Public Education). Also the supply by TRL/HA of the source data published in (Carder et al.[5]), and the climatic data provided by Icelandic Meteorological Office (for the city of Reykjavík) and by the meteorological station staff from the School of Engineering of the Autonomous University of Yucatan (for the city of Merida) is gratefully acknowledged.

Appendix

The following two analytical expressions for air temperature and solar radiation proposed by Cleall et al.[25] are used in this study. The expression for solar radiation is given by

$$R(t) = \frac{\pi}{2}\left(\cos^2(\gamma t) - \cos(\gamma t) + \frac{4-\pi}{2\pi}\right) \times (R_1 \cos(\varphi t) + R_2) \quad (14)$$

where t is given in seconds taking the origin at midyear (July 1st), φ is the annual period defined as $2\pi/31\,557\,600$ s, and γ is the daily period defined as $2\pi/86\,400$ s. R_1 and R_2 are coefficients, that can be determined from the experimental meteorological conditions for summer and winter. These coefficients are defined as

$$R_1 = 0.5(A - B) \quad (15)$$

$$R_2 = 0.5(A + B) \quad (16)$$

where A and B are the summer and winter daily average solar radiation respectively.

The expression for air temperature is given by

$$T_a(t) = T_1[\cos(\varphi t) + 0.5\sin(\varphi t)] + T_2 - \{T_3[\cos(\varphi t) + 0.5\sin(\varphi t)] + T_4\}\cos(\gamma t) \quad (17)$$

where t is given in seconds taking the origin at midyear (1st July). T_1, T_2, T_3 and T_4 are coefficients determined from the meteorological conditions for mid-summer and mid-winter periods. They are calculated as follows:

$$T_1 = 0.5(C - D) \quad (18)$$

$$T_2 = 0.5(C + D) \quad (19)$$

$$T_3 = 0.5(E - F) \quad (20)$$

$$T_4 = 0.5(E + F) \quad (21)$$

where coefficients C, D, E, and F are defined as the mid-summer daily average, mid-winter daily average, mid-summer average amplitude, and mid-winter average amplitude respectively.

References

[1] Florides G, Kalogirou S. Ground heat exchangers—A review of systems, models and applications. *Renew Energy*. 2007;32(15):2461–2478. http://dx.doi.org/10.1016/j.renene.2006.12.014.

[2] Wood CJ, Liu H, Riffat SB. An investigation of the heat pump performance and ground temperature of a piled foundation heat exchanger system for a residential building. In: *The 3rd International Conference on Sustainable Energy and Environmental Protection, SEEP 2009. Energy*. 2010;35(12):4932–4940. http://dx.doi.org/10.1016/j.energy.2010.08.032.

[3] Rees SW, Adjali MH, Zhou Z, Davies M, Thomas HR. Ground heat transfer effects on the thermal performance of earth-contact structures. *Renewable Sustainable Energy Rev*. 2000;4(3):213–265. http://dx.doi.org/10.1016/S1364-0321(99)00018-0.

[4] Zoras S. A review of building earth-contact heat transfer. *Adv Build Energy Res*. 2009;3(1):289–314. http://dx.doi.org/10.3763/aber.2009.0312.

[5] Carder DR, Barker KJ, Hewitt MG, Ritter D, Kiff A. Performance of an interseasonal heat transfer facility for collection, storage and re-use of solar heat from the road surface. Performance of an Interseasonal Heat Transfer Facility for Collection, Storage and Re-Use of Solar Heat from the Road Surface, Vol. 1, no. 1, 2007, pp. 1–114.

[6] Ma X, Cheng B, Liu W, Li J. Simulation and analysis on the initial temperature profiles in soils. In: *IEEE International Conference on Sustainable Energy Technologies, 2008. ICSET 2008*, 2008, pp. 253–256. http://dx.doi.org/10.1109/ICSET.2008.4747012.

[7] Qin Z, Berliner P, Karnieli A. Numerical solution of a complete surface energy balance model for simulation of heat fluxes and surface temperature under bare soil environment. *Appl Math Comput*. 2002;130(1):171–200. http://dx.doi.org/10.1016/S0096-3003(01)00089-3.

[8] Rajeev P, Chan D, Kodikara J. Ground–atmosphere interaction modelling for long-term prediction of soil moisture and temperature. *Can Geotech J*. 2012;49(9):1059–1073. http://dx.doi.org/10.1139/t2012-068.

[9] Liu C, Shi B, Tang C, Gao L. A numerical and field investigation of underground temperatures under Urban heat Island. *Build Environ*. 2011;46(5):1205–1210. http://dx.doi.org/10.1016/j.buildenv.2010.12.015.

[10] Yumrutaş R, Kanoğlu M, Bolatturk A, Bedir MŞ. Computational model for a ground coupled space cooling system with an underground energy storage tank. *Energy Build*. 2005;37(4):353–360. http://dx.doi.org/10.1016/j.enbuild.2004.07.004.

[11] Shang Y, Li S, Li H. Analysis of geo-temperature recovery under intermittent operation of ground-source heat pump. *Energy Build*. 2011;43(4):935–943. http://dx.doi.org/10.1016/j.enbuild.2010.12.017.

[12] Wu Y, Gan G, Verhoef A, Vidale PL, Gonzalez RG. Experimental measurement and numerical simulation of horizontal-coupled slinky ground source heat exchangers. *Appl Therm Eng*. 2010;30(16):2574–2583. http://dx.doi.org/10.1016/j.applthermaleng.2010.07.008.

[13] Esen H, Inalli M, Esen M. Numerical and experimental analysis of a horizontal ground-coupled heat pump system. *Build Environ*. 2007;42(3):1126–1134. http://dx.doi.org/10.1016/j.buildenv.2005.11.027.

[14] Inallı M, Esen H. Experimental thermal performance evaluation of a horizontal ground-source heat pump system. *Appl Therm Eng*. 2004;24(14–15):2219–2232. http://dx.doi.org/10.1016/j.applthermaleng.2004.01.005.

[15] Congedo PM, Colangelo G, Starace G. CFD simulations of horizontal ground heat exchangers: A comparison among different configurations. *Appl Therm Eng*. 2012;33–34(February):24–32. http://dx.doi.org/10.1016/j.applthermaleng.2011.09.005.

[16] Ramírez-Dávila L, Xamán J, Arce J, Álvarez G, Hernández-Pérez I. Numerical study of earth-to-air heat exchanger for three different climates. *Energy Build*. 2014;76(June):238–248. http://dx.doi.org/10.1016/j.enbuild.2014.02.073.

[17] Muñoz Criollo JJ. *An investigation of inter-seasonal near-surface ground heat transfer and storage* (Ph.D), Cardiff University; 2014:http://orca.cf.ac.uk/73226/.

[18] Cengel YA. *Heat Transfer: A Practical Approach*. 2nd ed. McGraw-Hill; 2003.

[19] Herb WR, Janke B, Mohseni O, Stefan HG. Ground surface temperature simulation for different land covers. *J Hydrol*. 2008;356(3–4):327–343. http://dx.doi.org/10.1016/j.jhydrol.2008.04.020.

[20] Jansson C, Almkvist E, Jansson P. Heat balance of an asphalt surface: Observations and physically-based simulations. *Meteorol Appl*. 2006;13(2):203–212. http://dx.doi.org/10.1017/S1350482706002179.

[21] North GR, Erukhimova TL. *Atmospheric Thermodynamics: Elementary Physics and Chemistry*. Cambridge University Press; 2009.

[22] Deardorff J. Efficient prediction of ground surface-temperature and moisture, with inclusion of a layer of vegetation. *J Geophys Res-Oceans Atmos*. 1978;83(NC4):1889–1903. http://dx.doi.org/10.1029/JC083iC04p01889.

[23] Best MJ. A model to predict surface temperatures. *Bound-Layer Meteorol*. 1998;88(2):279–306. http://dx.doi.org/10.1023/A:1001151927113.

[24] Cleall PJ, Muñoz-Criollo JJ, Rees SW. Assessment and representation of thermal surface fluxes in soils. In: *Computer Methods Recent Advances Geomechanics*. Kyoto, Japan: CRC Press; 2014:1321–1326, http://www.crcnetbase.com/doi/abs/10.1201/b17435-233.

[25] Cleall PJ, Muñoz-Criollo JJ, Rees SW. Analytical solutions for ground temperature profiles and stored energy using meteorological data. *Transp Porous Media*. 2014;106(1):181–199. http://dx.doi.org/10.1007/s11242-014-0395-3.

[26] Bangerth W, Hartmann R, Kanschat G. deal.II—a general-purpose object-oriented finite element library. *ACM Trans Math Softw*. 2007;33(4):http://dx.doi.org/10.1145/1268776.1268779. Article 24 (Preprint).

[27] UK Meteorological Office. Met Office Integrated Data Archive System (MIDAS) Land and Marine Surface Stations Data (1853-Current). NCAS British Atmospheric Data Centre. [Online], 2012. Available at: http://badc.nerc.ac.uk/view/badc.nerc.ac.uk__ATOM__dataent_ukmo-midas [Accessed: 03-Apr-2014].